

# Orbital Evolution of Impact Ejecta from Ganymede

Jose Luis Alvarellos

Space Systems/Loral, 3825 Fabian Way, MS L-27, Palo Alto, California 94303  
E-mail: alvarellos.jose@ssd.loral.com

Kevin J. Zahnle

NASA Ames Research Center, MS 245-3, Moffet Field, California 94035

Anthony R. Dobrovolskis

UCO/Lick Observatory, University of California, Santa Cruz, California 95064

and

Patrick Hamill

Department of Physics, San Jose State University, San Jose, California 95192

Received January 16, 2002; revised June 12, 2002

We have numerically computed the orbital evolution of  $\sim 10^3$  particles representing high-speed ejecta from Gilgamesh, the largest impact basin on Ganymede. The integration includes the four Galilean satellites, Jupiter (including  $J_2$  and  $J_4$ ), Saturn, and the Sun. The integrations last 100,000 years. The particles are ejected at a variety of speeds and directions, with the fastest particles ejected at 1.4 times the escape speed  $v_{\text{esc}} \equiv \sqrt{2GM_G/R_G}$  of Ganymede. Ejecta with speeds  $v < 0.96v_{\text{esc}}$  follow suborbital trajectories. At  $v \sim 0.96v_{\text{esc}}$  there is a transition characterized by complex behavior suggestive of chaos. For  $v > 0.96v_{\text{esc}}$ , most particles escape Ganymede and achieve orbits about Jupiter. Eventually most ( $\sim 71\%$ ) of the joventric particles hit Ganymede, with 92% of these hitting within 1000 years. The accretion rate scales as  $1/t$ . Their impact sites are randomly distributed, as expected for planetocentric debris. We estimate that most of the resulting impact craters are a few kilometers across and smaller. The rest of the escaping ejecta are partitioned as follows:  $\sim 3\%$  hit Io;  $\sim 10\%$  hit Europa;  $\sim 13\%$  hit Callisto; 2% reach heliocentric space; and less than  $\sim 1\%$  hit Jupiter. Only two particles survived the entire  $10^5$ -year integration. Ejecta from large impact events do not appear to be a plausible source of large craters on the Galilean satellites; however, such ejecta may account for the majority of small craters. © 2002 Elsevier Science (USA)

**Key Words:** cratering; Ganymede; satellites of Jupiter; orbits.

## I. INTRODUCTION

Impact craters on Ganymede are more isotropically distributed than would be expected if they were mostly made by comets falling from heliocentric orbits (Shoemaker and Wolfe 1982, Horedt and Neukum 1984, Zahnle *et al.* 2001); had this been the

case, we would expect to see 15- to 70-fold asymmetry between crater counts on the leading side vs the trailing side (Shoemaker and Wolfe 1982, Horedt and Neukum 1984, Zahnle *et al.* 2001). A similar statement could be made for almost every other satellite in the outer Solar System. With Ganymede and Europa one can reasonably argue that nonsynchronous rotation has occurred (Zahnle *et al.* 2001). For most other satellites one can plausibly argue that the isotropy implies that the craters are saturated—meaning that on average each new crater destroys an older crater (Lissauer *et al.* 1988). A case can be made that crater saturation and slow nonsynchronous rotation can, between them, account for the distribution of larger craters in the outer Solar System (Zahnle *et al.* 2001).

A competing explanation, that many of the impact craters in the outer Solar System have planetocentric origins, has been at least as popular (Strom *et al.* 1990). By planetocentric one means that the impacting bodies were themselves satellites of the planet in orbits akin to those of the satellites that remain. Craters made by such a population are isotropically distributed across the surface of a prograde, synchronously locked satellite (Horedt and Neukum 1984). They can help explain what we see in the outer satellites by diluting the expected asymmetry. Collisional lifetimes of planetocentric bodies are expected to be extremely short if their orbits cross those of the massive satellites. Because planetocentric material is swept up quickly (time scales of  $\sim 10$  to  $\sim 10^3$  years), it is unlikely that many of the craters we see now have anything to do with a surviving remnant of a primordial planetocentric population. What is required rather is a mechanism of planetocentrogenesis: some means of creating fresh populations of planet-orbiting debris.

This was recognized by Shoemaker (Smith *et al.* 1982), who argued that satellites in the outer Solar System were subject to collisional disruption and reaccretion. This might have occurred several times for some of the smaller innermost satellites, which are the most vulnerable for a variety of reasons (Zahnle *et al.* 2001).

A related source for planetocentric impactors in the modern Solar System are ejecta from large impact events. Impact velocities of heliocentric bodies (e.g., comets) on satellites in the outer Solar System are usually at least an order of magnitude higher than the escape velocity and often several orders of magnitude higher (e.g., impact velocities on Mimas are on the order of  $25 \text{ km s}^{-1}$ , while the escape velocity is  $0.16 \text{ km s}^{-1}$ ). Under such conditions much of the ejecta generated by the excavation of the primary crater is launched faster than the classical two-body escape speed and so goes into orbit about the planet. Ultimately most of this material falls back onto the satellites to make craters. Thus we may regard this class of planetocentric cratering as an exalted form of secondary cratering.

This paper addresses the fate of impact ejecta in the Galilean satellite system. We take as a test case the young Gilgamesh impact basin on Ganymede. Gilgamesh is  $\sim 600 \text{ km}$  in diameter and located at  $58^\circ$  South and  $237^\circ$  East. It is on the leading hemisphere. Elsewhere one of us estimated that the Gilgamesh impact ejected  $10^{18} \text{ kg}$  of material,  $1/10$  of which escaped Ganymede (Zahnle *et al.* 2001). We use Levison and Duncan's (1994) SWIFT-RMVS3 integrator to follow test particles ejected from Gilgamesh at velocities comparable to and greater than Ganymede's escape velocity. In Section II we briefly review previous work related to this topic. In Section III we describe the initial conditions in detail. In Section IV we discuss the dynamical evolution and fates of the ejecta particles. In Section V we consider impacts on the Galilean satellites by planetocentric debris (with an emphasis on Ganymede). Finally in Section VI we summarize our findings and state our conclusions.

## II. PREVIOUS WORK

Motivated by the existence of lunar meteorites, Gladman *et al.* (1995) studied the dynamics of lunar impact ejecta. In their study, most particles were radially ejected from the Moon's surface with speeds comparable to the (classical) lunar escape speed  $v_{\text{esc}} = 2.38 \text{ km s}^{-1}$ . A few particles were launched somewhat faster. The top speed was  $3.5 \text{ km s}^{-1}$ . The particles were followed for up to  $10^6$  years. Gravitational perturbations of all the planets out to Saturn were included. Gladman *et al.* found that, for material ejected very close to the escape speed, 88% of the particles escaped to heliocentric space, about 9% hit the Moon, and 3% struck the Earth. The percentage striking the Moon decreased monotonically as the ejection speed increased, while the fraction that hit the Earth rose to a peak of 20% at  $v \sim 2.6\text{--}2.8 \text{ km s}^{-1}$ , then fell to zero as the speed approached  $3.5 \text{ km s}^{-1}$ . Gladman *et al.* (1995) showed that, to reproduce the observed distribution of lunar meteorite transfer ages, the speed distribu-

tion of the impact ejecta must be very steep—fewer than half could have been launched at more than  $1.25v_{\text{esc}}$ .

Gladman (1997) and Mileikowsky *et al.* (2000) investigated the dynamics of impact ejecta launched from Mars. Ejection speeds were again kept close to the escape speed (here  $5.3 \text{ km s}^{-1}$ ). Gladman (1997) found that for particles ejected near the escape speed, about 10% hit Mars and another 10% hit the Sun, while smaller fractions hit Earth, Venus, and Jupiter (between 2 and 3%). At higher launch speeds ( $\sim 6 \text{ km s}^{-1}$ ) the fraction of particles hitting the Sun rose slightly to 14% while the fraction hitting Mars dropped to less than 1%. More particles hit Earth, Venus, and Jupiter (5–6%). Mileikowsky *et al.* (2000) were concerned with transfer of viable organisms from Mars to Earth. They give prompt transfer rates but not total transfer efficiencies.

Concern for the safety of the *Cassini* spacecraft prompted Burns and Gladman (1998) to undertake a preliminary test particle survey of the Saturn system. As part of their investigations, they also studied the fate of ejecta from Mimas. In that experiment, they ejected 100 randomly placed particles radially outward at  $100 \text{ m s}^{-1}$  and another 100 at  $500 \text{ m s}^{-1}$ . Particles were ejected not from the surface but from 100 Mimas radii away. They found that Mimas is very efficient at reaccreting its own ejecta, as half the material reaccumulated in about 50 years. Dobrovolskis *et al.* (2000) have carried out a similar test particle survey of the Galilean satellite system, but they did not include ejecta from the jovian moons.

Farinella *et al.* (1983, 1990) have performed semianalytical calculations of the fates of ejecta from Saturn's small moon Hyperion. They concluded that such debris would be quantitatively accreted by Hyperion's massive neighbor Titan, rather than scattered throughout the Saturn system. Later numerical integrations (Farinella *et al.* 1997) appeared to bear this out, at least over their 5000-year time span. However, more recent numerical simulations over 100,000 to 200,000 years (Dobrovolskis and Lissauer 2000) have revealed that a substantial fraction of Hyperion ejecta eventually crosses the orbits of all of Saturn's moons, even impacting the planet itself as well as its rings.

## III. INITIAL CONDITIONS

The initial conditions for the massive bodies were obtained from the JPL ephemeris and correspond to the epoch JDE 2448896.5 (Oct. 1.0, 1992), jovian mean equator of date. The massive bodies included in the integration are Jupiter plus its oblateness terms  $J_2$  and  $J_4$ , the four Galilean satellites, Saturn, and the Sun. To obtain initial conditions for the ejecta we assign to each particle initial positions and velocities in a body-fixed coordinate system. Then we transform these initial conditions to the jovicentric frame (presumed to be inertial) in which the positions and velocities of the massive bodies are expressed. Details can be found in Bate *et al.* (1971) and other textbooks.

The physics of ejecting material out of a crater during an impact event are complex (Cintala *et al.* 1979, Chapman and

**TABLE I**  
**Adopted Numerical Data**

Item	Value
Jupiter mass, $M_J$	$1898.6 \times 10^{24}$ kg
Jupiter radius, $R_J$	71,398 km
Jupiter oblateness terms ( $J_2, J_4$ )	0.014736, $-0.0000587$
Ganymede mass, $M_G$	$1482 \times 10^{20}$ kg
Ganymede radius, $R_G$	2634 km
Ganymede escape speed, $v_{\text{esc}}$	$2.740 \text{ km s}^{-1}$
Ganymede semimajor axis, $a_G$	$1.070 \times 10^6$ km ( $14.99 R_J$ )
Ganymede orbital period	7.155 days
Ganymede rotational period	7.155 days
Ganymede inclination	$0.195^\circ$
Ganymede eccentricity	0.0015 (forced)
Approx. orbital speed of Ganymede	$10.88 \text{ km s}^{-1}$
Gilgamesh latitude, $\phi$	$-58^\circ$
Gilgamesh East longitude, $\lambda$	$237^\circ$

*Note.* From Murray and Dermott (1999).

McKinnon 1986, Melosh 1989). Here we ignore complexities and assume that for very energetic impacts, some material will get ejected at very high speeds and some will escape. The parameters we need in the body-fixed frame are the particle's initial speed  $v$  and its direction, in the form of azimuth  $\alpha$  and zenith angle  $\zeta$  (measured from the local vertical). Since we are mainly concerned with ejecta that escape Ganymede, we concentrate on speeds close to escape speed. We eject several rings, each containing 60 particles, and each differing from the others in the zenith angle and ejection speed. It is convenient to express the ejection speed as

$$v = f v_{\text{esc}}, \quad (1)$$

where  $v_{\text{esc}} = \sqrt{2GM_G/R_G} = 2.74 \text{ km s}^{-1}$  is the classical, two-body escape speed from Ganymede and  $f$  is a dimensionless factor. The slow rotation of Ganymede does not appreciably affect the motion of particles moving close to the escape speed. Ganymede's period of rotation is  $P_G = 7.155$  days, so that the speed of a particle launched from latitude  $\phi$  is approximately  $27 \cos \phi \text{ m s}^{-1}$ , which is always less than 1% of Ganymede's escape speed (see the Appendix for a more thorough discussion of the effect of rotation on the particles' speed).

The speed distribution of impact ejecta is often represented as a power law of the form  $N(v) dv = C v^{-q} dv$ ; various authorities have used different values for the exponent  $q$ , but all of them assume a sharp drop off in high speeds ( $2 \leq q \leq 10$ ; see Gault *et al.* 1963, Burns *et al.* 1984, Wetherill, 1984, Farinella *et al.* 1994). This power-law distribution and the lunar studies of Gladman *et al.* (1995) suggest that relatively few ejecta are launched much faster than the escape speed. For the ring ejecta, we use speeds  $0.96 \leq f \leq 1.40$  and discrete zenith angles  $\zeta = 30^\circ, 45^\circ, \text{ and } 60^\circ$ . In addition, we also launched 167 test particles radially ( $\zeta = 0^\circ$ ) from a position 1 km above the

center of Gilgamesh at speeds uniformly distributed in the range  $0.90 \leq f \leq 1.40$ . We then convert the velocities of the test particles from the body-fixed frame into the jovicentric coordinate system so that we can integrate the ejecta particles along with the massive bodies. Table I summarizes the relevant numeric data.

#### IV. DYNAMICAL EVOLUTION AND FATE OF THE TEST PARTICLES

We integrate the system for 100,000 years using the SWIFT numerical integration package of Levison and Duncan (1994); we used their regularized, mixed variable symplectic (RMVS3) integrator. This program implements an algorithm initially devised by Wisdom and Holman (1991). SWIFT removes a test particle from the integration for any of the following reasons: (a) it finds that the particle is too close to a massive body (closer than one planetary radius); (b) it predicts that the particle will crash in the next step; or (c) it finds the particle's periape distance to be less than one planetary radius. We also set up the program to (d) remove a particle from the integration if it escapes into heliocentric space, i.e., if its distance from Jupiter exceeds one Jupiter Hill radius ( $53.2 \times 10^6$  km or 0.355 AU). We present four case studies, each case with different sets of initial conditions for the test particles; we pay particular attention to the case of radial ejection.

##### *Case 1: Radial Ejecta*

We ejected 167 test particles radially away from Gilgamesh ( $\zeta = 0^\circ$ ) with speeds uniformly distributed in the range  $0.90 \leq f \leq 1.40$ . Results are summarized in Table II. It is obvious at a glance that most (114 particles, or 68% of the total) of the particles strike Ganymede. In Fig. 1 we plot the survival times and fates of the radial ejecta as a function of the ejection speed  $f$ . Different symbols represent the different fates. The regular curve at low speeds ( $f < 0.95$ ) is drawn by the 18 slowest particles. They executed suborbital trajectories that fell back to Ganymede between 0.42 and 1.3 days. Their impact sites form a regular pattern, as we will see in Section V. There appears

**TABLE II**  
**Fate of the Ejected Test Particles for the (Radial) Case  $\zeta = 0^\circ$ ,  $0.90 \leq f \leq 1.40$**

Fate	Number of particles	% of total
Hit Jupiter	0	0.00
Hit Io	3	1.80
Hit Europa	18	10.78
Hit Ganymede	114	68.26
Hit Callisto	26	15.57
Heliocentric <sup>a</sup>	6	3.59
Survivors	0	0.00
Total	167	100.00

<sup>a</sup> By heliocentric we mean that the particle has escaped beyond Jupiter's Hill sphere.

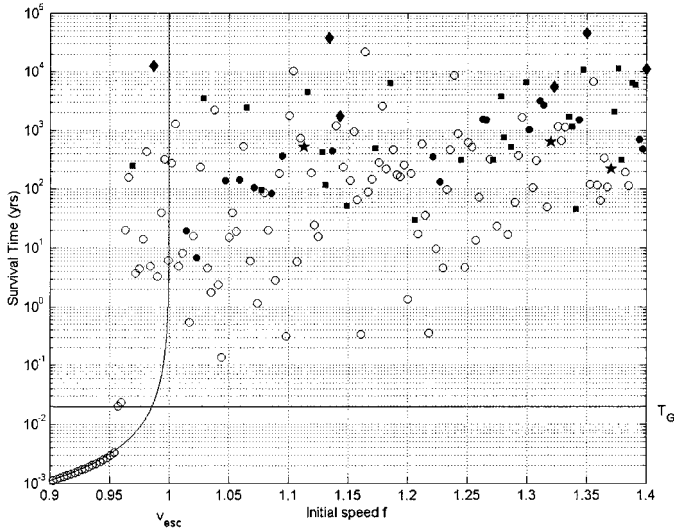


**FIG. 1.** Survival time vs initial speed  $f$  for Case 1 ( $\zeta = 0^\circ$ ). The horizontal line labeled  $T_G$  represents one Ganymede period. The regular pattern at low speeds is produced by ejecta traveling on suborbital trajectories. There is a transition at  $f \sim 0.96$ , beyond which particles are able to escape to joventric space. The smooth curve is given by the time-of-free-flight formula (Eq. (2)). The first 18 particles stay close to the predicted curve because they undergo suborbital trajectories and impact Ganymede in times ranging from 0.42 to 1.3 days after launch. The two objects impacting close to  $T_G$  represent transition objects. Ganymede impacts are hollow circles (114 cases); all other fates are represented by filled symbols. Io impacts are solid stars (3 cases). Europa impacts are solid circles (18 cases). Callisto impacts are solid squares (26 cases). Heliocentric escape is shown by solid diamonds (6 cases). All particles are removed by  $t = 45,117$  years.

to be a threshold value at  $f \sim 0.96$  above which particles exhibit more complicated behavior; in fact, some particles with speeds less than the classical escape speed are able to achieve joventric orbits. This occurs because of the gravitational influence of Jupiter, which becomes important when a particle's trajectory brings it to Ganymede's Hill radius  $R_H$ . We show in the Appendix that the critical speed for particles ejected radially from the surface is  $f_c = 0.9576$  ( $2.623 \text{ km s}^{-1}$ ). To see how well this prediction agrees with our simulations, we compare the impact time of ejecta with a formula for the impact time derived from two-body dynamics, the time-of-free-flight formula (Dobrovolskis 1981, or see Bate, *et al.* 1971, p. 293)

$$T_{\text{ff}} = 2\sqrt{\frac{a^3}{GM_G}}(\pi - E_1 + e \sin E_1), \quad (2)$$

where  $a$  and  $e$  are the initial semimajor axis and eccentricity of the ejected particle with respect to Ganymede, and  $E_1$  is the eccentric anomaly of the initial point, obtained from

$$\cos E_1 = \frac{R_G v_o^2}{eGM_G} - \frac{1}{e} \approx \frac{2f^2 - 1}{(1 + 4f^2(f^2 - 1)\sin^2 \zeta)^{1/2}} \quad (3)$$

( $v_o$  is the particle's inertial launch speed; see the Appendix). The impact time computed using Eq. (2) is shown in Fig. 1 as the smooth curve that tends to infinity as  $f$  approaches unity. The disagreement with two-body dynamics is very strong past the critical value. One particle with  $f = 0.969$  not only achieved a joventric orbit, but it reached Callisto 252 years after launch (shown in Fig. 1 as the leftmost solid square).

With the exception of the low-speed suborbital particles, there does not appear to be any strong correlation between a particle's fate and its ejection speed (Fig. 1), although the probability of impacting Ganymede appears to decrease slightly at faster speeds. Of the 167 particles ejected radially from Gilgamesh, 53 did not impact Ganymede: 26 hit Callisto, 18 hit Europa, 6 escaped, 3 hit Io, and none hit Jupiter. No particles remained in orbit about Jupiter at the end of the integration. The last survivor escaped 45,117 years after it was launched. Collisions with Europa and Callisto usually occur on time scales of several hundred years. However, inter-satellite exchanges of material can occur quickly: in one case, a particle ejected radially at a speed of  $f \sim 1.02$  arrived at Europa in 6.8 years. In contrast, all the particles that escaped took thousands or tens of thousands of years to do so.

There are two particles in Fig. 1 which hit Ganymede 7.3 and 8.5 days after launch respectively ( $f = 0.957$  and  $0.960$ ). The impact times are close to the orbital period of Ganymede ( $P_G = 7.155$  days). These two particles represent a transition between suborbital and joventric orbits. The behavior of ejecta with speeds close to the critical value  $f_c$  is so interesting that we decided to do an additional high-resolution simulation consisting of 50 particles ejected radially with speeds uniformly distributed between  $f = 0.94$  and  $0.98$ . The output interval from SWIFT was kept small (30 min) to capture the dynamics occurring in short time scales, while the duration of the integration was kept short to only 100 days. In this numerical experiment we found three distinct modes of behavior. For  $f \lesssim 0.960$ , particles follow suborbital trajectories, as expected. For  $f \gtrsim 0.964$ , particles enter joventric orbits, also as expected. But for intermediate values of  $f$ , particles just reach the Hill sphere and either remain on suborbital paths or else become temporary satellites of Ganymede! Note that this choice is not a monotonic function of  $f$ .

These three behaviors are easily distinguished in Fig. 2, which shows the greatest distance  $\rho_{\text{max}}$  a particle attained from the center of Ganymede versus the time  $T_{\text{max}}$  after launch at which that maximum was reached. The horizontal and vertical dotted lines indicate the period and diameter ( $2a_G = 2.140 \times 10^6$  km) of Ganymede's orbit, respectively, while the dashed vertical line designates Ganymede's Hill radius  $R_H$ . The crosses denote particles which collided with Ganymede, while the open circles represent particles which were still active at the end of the simulation at 100 days after launch. The crosses with  $T_{\text{max}} < 1$  day,  $\rho_{\text{max}} \lesssim R_H$  correspond to suborbital particles, with  $f \leq 0.9592$  as well as  $f = 0.9608$  and  $0.9616$ . The circles with  $T_{\text{max}} > 20$  days,  $\rho_{\text{max}} \sim 2a_G$  indicate particles with  $f \geq 0.9640$  which have entered joventric orbits. However, the three crosses

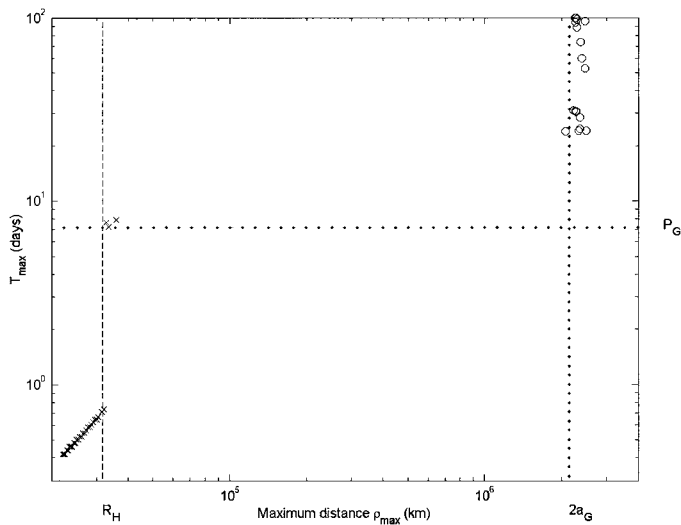


**FIG. 2.** Abscissa: the greatest distance  $\rho_{\max}$  a particle attained from the center of Ganymede in 100 days. Ordinate: the time  $T_{\max}$  after launch at which that maximum was reached. The horizontal and vertical dotted lines indicate the period and diameter of Ganymede's orbit; the dashed vertical line designates Ganymede's Hill radius  $R_H$ . The crosses denote particles which collided with Ganymede, while the open circles plot particles which were still active 100 days after launch. The crosses with  $T_{\max} < 1$  day,  $\rho_{\max} \lesssim R_H$  correspond to suborbital particles. The points with  $T_{\max} > 20$  days,  $\rho_{\max} \sim 2a_G$  indicate particles that have entered joventric orbits. The three crosses with  $T_{\max} \sim P_G$ ,  $\rho_{\max} \sim R_H$  designate particles which became temporary satellites of Ganymede.

with  $T_{\max} \sim P_G$ ,  $\rho_{\max} \sim R_H$  designate particles with  $f = 0.9600$ ,  $0.9624$ , and  $0.9632$ , which became temporary satellites of Ganymede.

In Fig. 3 we show the orbit with respect to Ganymede of the particle with  $f = 0.9600$  also shown in Figs. 1 and 2; the orbit is quite distorted by strong gravitational perturbations from Jupiter. The particle's path began as a nearly straight line until it was pulled back to Ganymede; after that it followed a strongly perturbed, high-eccentricity polar orbit until the particle impacted 8.5 days after launch. Orbits of this kind are entirely due to strong third-body gravitational perturbations. In the two-body problem only suborbital ( $f < 1.0$ ) or hyperbolic/escape ( $f \geq 1.0$ ) orbits are possible.

*Case 2:  $\zeta = 30^\circ$ ;  $f = 0.96, 0.98, 1.00, 1.20, 1.40$*

In this case, we launched rings of ejecta at five different speeds, all with the same zenith angle  $\zeta = 30^\circ$ . Each ring had 60 particles uniformly distributed in azimuth for a total of 300 particles. The speeds of the particles were set at the discrete values  $f = 0.96, 0.98, 1.00, 1.20$ , and  $1.40$ ; we adopt as the lowest ejection speed the approximate critical value found in the radial case. We summarize our findings in Table III. As in Case I, most of the particles (223 of 300, or 74%) hit Ganymede. Of these, 28 hit within one Ganymede period from launch (7.155 days). Of the particles that did not hit Ganymede, more than half (41 of 77) hit Callisto. The incidence of Jupiter impacts and escapes into

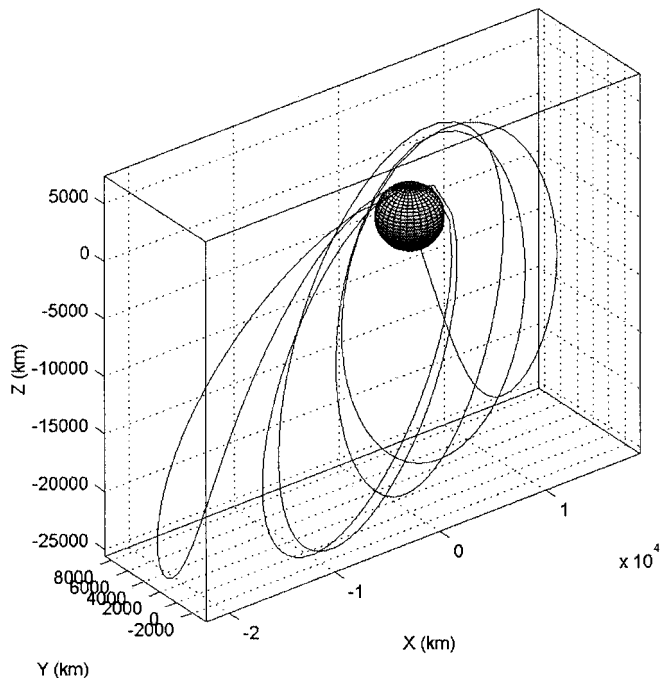


**FIG. 3.** The orbit with respect to Ganymede of a particle ejected radially at  $f = 0.960$ . This particle became a temporary satellite before impacting 8.5 days after launch (shown in Fig. 1 as the higher open circle just above the horizontal line representing  $T_G$ ). Ejecta of this type represent a transition between the low-energy, suborbital trajectories and the high-energy, joventric orbits. The Hill radius is 31,706 km.

heliocentric space were low (2 and 3 particles, respectively), as in the previous case study. One particle survived in orbit about Jupiter at the end of the  $10^5$ -year simulation.

*Case 3:  $\zeta = 45^\circ$ ;  $f = 0.96, 0.98, 1.00, 1.20, 1.40$*

This is the same as Case 2 but with  $\zeta = 45^\circ$ . We summarize our findings in Table IV. As before, most of the particles impacted Ganymede. Again Europa and Callisto were hit more often than the more distant targets. Only one particle was left

**TABLE III**  
Fate of Ejecta for the Case  $\zeta$  (Zenith Angle) =  $30^\circ$  at Five Different Speeds

Fate	$f$					Total	% of total
	0.96	0.98	1.00	1.20	1.40		
Hit Jupiter	0	0	2	0	0	2	0.67
Hit Io	1	1	1	6	1	10	3.33
Hit Europa	3	3	3	3	8	20	6.67
Hit Ganymede	52	50	47	35	39	223	74.33
Hit Callisto	4	6	7	15	9	41	13.67
Heliocentric	0	0	0	1	2	3	1.00
Survivors	0	0	0	0	1	1	0.33
Total	60	60	60	60	60	300	100.00

TABLE IV  
Fate of Ejecta for the Case  $\zeta$  (Zenith Angle) =  $45^\circ$  at Five Different Speeds

Fate	$f$					Total	% of total
	0.96	0.98	1.00	1.20	1.40		
Hit Jupiter	0	1	0	0	0	1	0.33
Hit Io	1	1	1	3	1	7	2.33
Hit Europa	3	8	5	7	10	33	11.00
Hit Ganymede	55	49	45	40	34	223	74.33
Hit Callisto	1	1	7	10	10	29	9.67
Heliocentric	0	0	1	0	5	6	2.00
Survivors	0	0	1	0	0	1	0.33
Total	60	60	60	60	60	300	100.00

orbiting Jupiter at the end of the simulation (more will be said about this and the survivor in Case 2 later).

Case 4:  $\zeta = 60^\circ$ ;  $f = 0.96, 0.98, 1.00, 1.20, 1.40$

This is the same as Cases 2 and 3 except that  $\zeta = 60^\circ$ . We summarize our findings in Table V. At  $f = 1.20$  there was one particle that SWIFT decided to remove from the integration because of an apparent collision with Ganymede. When we checked where this test particle would hit with our own program (see Section V), it showed that the particle grazed Ganymede and then escaped its Hill sphere. The discrepancy may be due to the simplifications we made in our program; however, since the closest approach to Ganymede was so small (229 m above the surface) we will count this case as a “hit.” Again the majority of the ejected particles impacted Ganymede. No particles hit Jupiter and no particles survived.

#### Summary and Discussion of the Four Case Studies

By combining the results of the material ejected radially (Case 1) and the cases of the ejected particles at zenith angles  $\zeta = 30^\circ, 45^\circ$ , and  $60^\circ$  (Cases 2, 3, and 4 respectively) we hope to present a realistic picture of the fate of fast ejecta in the jovian system. We note that the cases ejected at nonzero angles (900 par-

TABLE V  
Fate of Ejecta for the Case  $\zeta$  (Zenith Angle) =  $60^\circ$  at Five Different Speeds

Fate	$f$					Total	% of total
	0.96	0.98	1.00	1.20	1.40		
Hit Jupiter	0	0	0	0	0	0	0.00
Hit Io	0	1	0	2	5	8	2.67
Hit Europa	2	4	5	9	7	27	9.00
Hit Ganymede	52	52	45	41	37	227	75.67
Hit Callisto	6	3	9	8	6	32	10.67
Heliocentric	0	0	1	0	5	6	2.00
Survivors	0	0	0	0	0	0	0.00
Total	60	60	60	60	60	300	100.00

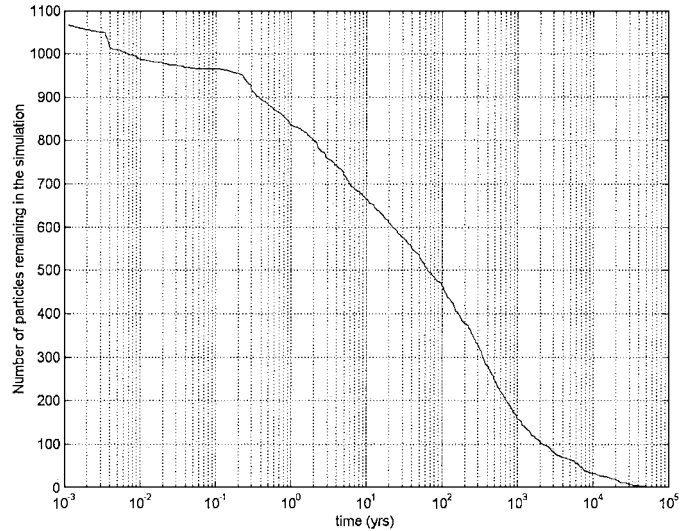
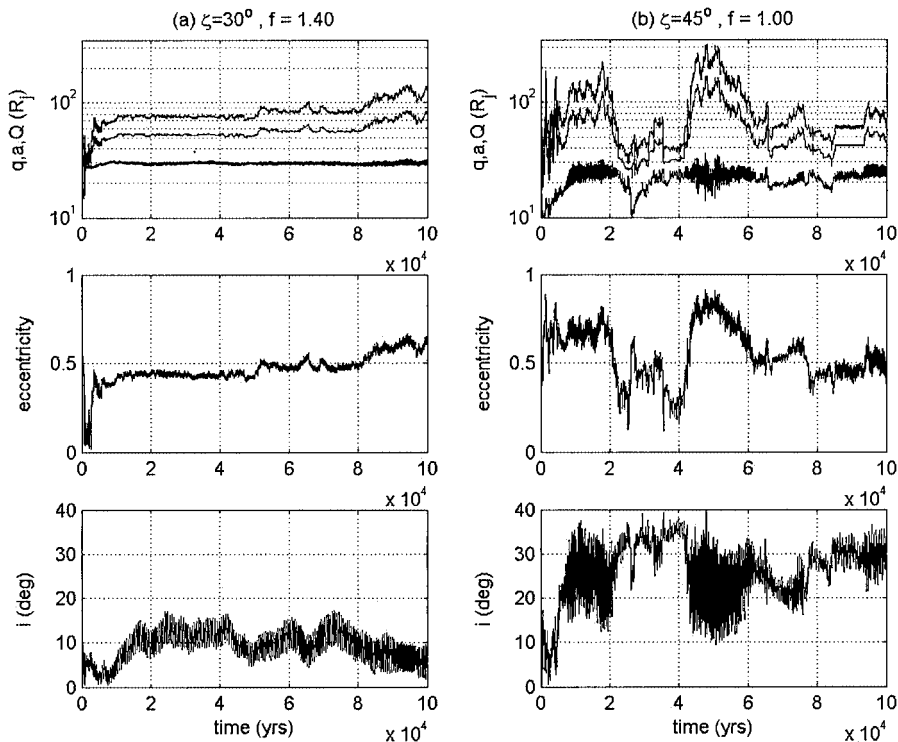


FIG. 4. Number of ejecta particles remaining as a function of time. Note the logarithmic scale on the time axis. Nearly three-quarters of the ejecta particles (787 out of 1067) are reaccruted by Ganymede; the rest are removed by impacts into the other Galilean satellites (254) or Jupiter (3), while some escape to heliocentric space (21). Only two particles remained at the end of the simulation.

ticles at the discrete speeds  $f = 0.96, 0.98, 1.00, 1.20$ , and  $1.40$ ) cover different speeds than the radial ejecta ( $167$  particles with  $0.90 \leq f \leq 1.40$ ). In Fig. 4 we plot the number of particles remaining as a function of time. We start with all  $1067$  particles, and only two particles remain in orbit about Jupiter after  $10^5$  years. Notice that the decay rate is different in different time scales, a fact which indicates that there are different dynamical regimes at work here. That we see a nearly straight line in Fig. 4 during part of the simulation (roughly in the span  $10^{-1} < t < 10^3$  years) indicates a logarithmic decay of the particle population. Evans and Tabachnik (1999), who investigated the possible existence of long-lasting asteroid belts in the inner Solar System, also found that the number of test particles remaining as a function of time in certain regions of the inner Solar System follow logarithmic-type decay. We will look at some specific particle time histories next.

Consider first the two particles that remained in orbit around Jupiter at the end of the simulation. The first of these was launched at  $\zeta = 30^\circ$  and  $f = 1.40$ . For the first  $10,000$  years its orbit is very irregular (Fig. 5a). Then, from  $10,000$  to  $50,000$  years, its orbit acquires a semblance of regularity: its average semimajor axis during this period hovers around  $53 R_J$ , while the average eccentricity lies around  $0.45$  and inclination (referred to Jupiter’s equator) lies in the range  $5^\circ < i < 13^\circ$ . At  $t \sim 50,000$  years the particle’s orbit regains some of its previous irregular qualities, and at  $t \sim 81,000$  years the semimajor axis and eccentricity start to grow, while the inclination decreases somewhat: at the end of the simulation,  $a \sim 82 R_J$ ,  $e \sim 0.63$ , while  $i \sim 6^\circ$ . It is worth noting how stable the periape distance  $q = a(1 - e)$  remains during the simulation. For the period  $10,000 < t < 100,000$  years, the average periape distance  $\langle q \rangle \sim 29.9 R_J$  with a standard



**FIG. 5.** Time histories of the semimajor axis, eccentricity, and inclination for the only two particles that remained in orbit about Jupiter at the end of the 100,000-year integration. Note also the logarithmic scales in the semimajor axes. (a) This particle was launched at a zenith angle of  $30^\circ$  and a speed of  $f = 1.40$ ; since the semimajor axis is increasing toward the end of the simulation, the most likely long-term fate of this particle is escape to heliocentric space due to increasing solar tides. (b) This particle was launched at a zenith angle of  $45^\circ$  and a speed  $f = 1.00$ ; its motion is highly irregular throughout the integration. The most likely long-term fate is a collision with Callisto or a close encounter with it which would expel it from the jovian system. Note that the same scale for  $a$ ,  $e$ , and  $i$  is used on both plots.

deviation of only  $0.7 R_J$ . The minimum periaapse distance during this same interval was  $28.1 R_J$ , which translates into a minimum distance between this particle and Callisto of  $r_{\min} \sim 1.7 R_J$ . Since the semimajor axis is fairly large and growing at the end of the simulation, solar perturbations will become increasingly important in its future.

The other survivor was launched at  $\zeta = 45^\circ$  and  $f = 1.00$  (Fig. 5b). Its orbit is highly irregular throughout the whole integration. The eccentricity spans  $0.1 < e < 0.9$ , while the inclination spans  $0^\circ < i < 40^\circ$ . The semimajor axis is large and its variations are pronounced, indicating strong solar perturbations. At 48,000 years the apoapse distance  $Q$  reached  $\sim 310 R_J$ , almost halfway to Jupiter's Hill radius, which is roughly the stability limit for prograde orbits (Hamilton and Burns 1991). By  $t \sim 65,000$  years, however, the semimajor axis shrinks substantially, with the particle getting temporarily trapped in a 1 : 2 mean motion resonance with Callisto during  $85,000 < t < 93,000$  years (when its average semimajor axis was approximately  $41.8 R_J$ ). During the last 10,000 years, the periaapse distance  $q$  averaged  $\sim 24.5 R_J$ , which means that the near future evolution of this particle will be controlled by Callisto, which has a semimajor axis of  $26.3 R_J$ .

A small fraction of particles became minor planets in their own right (21 cases). A typical example is presented in Fig. 6.

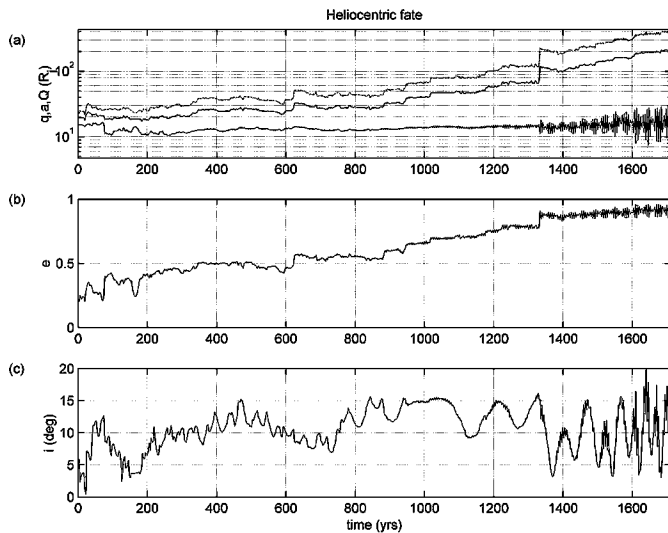


**FIG. 6.** Time history for a particle that reached heliocentric space. This particle was ejected radially at a speed of  $f = 1.143$  and was removed from the integration  $\sim 1713$  years after launch. (a) Perijove, semimajor axis and apoapse distance. While  $q$  stays relatively constant ( $(q) \sim 14 R_J$ ),  $a$  and  $Q$  grow rapidly; note the log scale on the y axis. (b) Eccentricity; it grows roughly linearly. (c) Inclination from Jupiter's equator.

The behavior of the perijove distance  $q$  is interesting in that it is fairly constant during the whole integration; its mean value is  $13.8 R_J$ , close to Ganymede's semimajor axis ( $15.0 R_J$ ), while the eccentricity grows roughly linearly. This particle saw three close approaches to Ganymede at  $t \sim 74$  years,  $t \sim 620$  years, and most noticeably at  $t \sim 1330$  years. The particle's distance from Jupiter became greater than a Jupiter Hill radius at  $t = 1,711$  years, at which point we removed it from the simulation. We have observed that the three particles that hit Jupiter have orbits similar to the escape shown in Fig. 6, save that eccentricities reached unity before the semimajor axis grew larger than Jupiter's Hill radius.

We have found it useful to plot the cumulative number of hits on each moon as a function of time. In Fig. 7 we show the cumulative number of impacts on each Galilean satellite (except Ganymede) as a function of time. After  $10^5$  years, Io had received 28 impacts, while Europa and Callisto received 98 and 128 impacts respectively. The Europa and Callisto curves are fairly similar: except for the beginning and end of the integration, the cumulative number of impacts from jovian objects seems to increase roughly logarithmically. Note how after a certain time scale (roughly between 1000 and 3000 years), the number of hits on Io and Europa began to taper off, as if reaching some asymptotic limit; there are few particles left to accumulate. The number of impacts on Callisto seems to increase with only a slight sign of tapering off after  $t \sim 7000$  years. The cumulative number of impacts is higher on Europa than on Callisto until about  $t \sim 2000$  years. The first impact on Europa occurred only 2.5 years after launch, which was the shortest time we found to transfer material from Ganymede to another body. While the

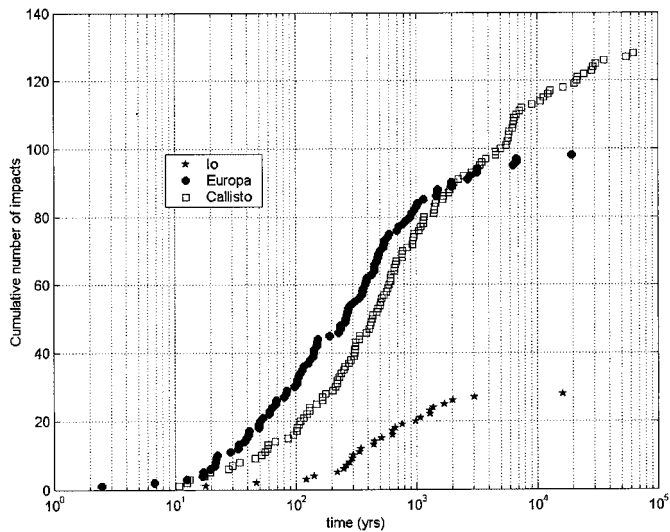


FIG. 7. Cumulative number of impacts on Io, Europa, and Callisto as a function of time. Note the logarithmic scale on the time axis. Io received a total 28 impacts, while Europa and Callisto received 98 and 128 impacts respectively. The number of impacts seems to increase logarithmically up to a certain time, then begin to taper off. The exception is Callisto, which shows no strong sign of leveling off.

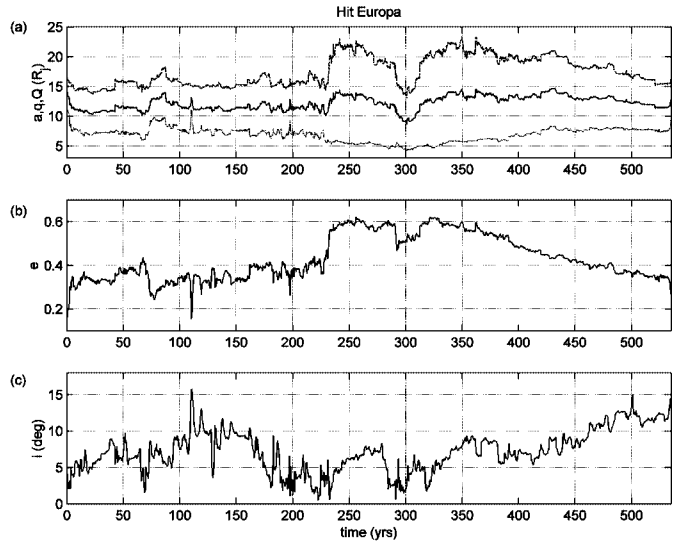


FIG. 8. Time history for a particle that hit Europa. This particle was ejected at  $\zeta = 45^\circ$  and at a speed  $f = 1.20$  and hit Europa  $\sim 535$  years after launch. (a) Perijove, semimajor axis, and apojove distance. (b) Eccentricity. (c) Inclination from Jupiter's equator.

last impacts on Io and Europa occurred 16,200 and 19,300 years after launch from Gilgamesh respectively, Callisto continued to sweep up ejecta until  $t \sim 62,500$  years.

In Fig. 8 we show the history of a particle that hit Europa. The semimajor axis varied chaotically between  $8.7$  and  $16.4 R_J$ . The minimum  $q$  was  $4.2 R_J$ , while the maximum  $Q$  was  $23.4 R_J$ , so this particle could have closely approached any of Io, Europa, or Ganymede. It is useful at this point to review some of the reasons for orbital chaos more closely. Expanding on Chirikov's work (1979), Wisdom (1980) derived the concept of a "chaotic zone," a band of semimajor axes surrounding a satellite where many high-order resonances between the particle and satellite overlap. The lower and upper boundaries of this chaotic zone are given by (Duncan *et al.* 1989)

$$a = a_s \left[ 1 \pm 1.49 \left( \frac{M_s}{M_J} \right)^{2/7} \right], \quad (4)$$

where  $a_s$  is the satellite's semimajor axis, while  $M_s$  and  $M_J$  are the masses of the satellite and Jupiter respectively. Mean motion resonances with the Galilean satellites can also drive an otherwise stable orbit to chaos. This specific particle did not get trapped into any obvious long-lasting resonances, although its semimajor axis made several brief incursions into the chaotic zones of Europa (spanning from  $8.7$  to  $10.1 R_J$ ) and Ganymede (spanning from  $13.5$  to  $16.5 R_J$ ). It finally hit Europa at  $t = 535$  years.

In Fig. 9 we show a particle that hit Callisto. This particle was in turn trapped in several different resonances. First it fell into a  $2:3$  resonance with Ganymede from approximately  $45 < t < 165$  years (average semimajor axis  $\langle a \rangle \sim 19.7 R_J$ ), with

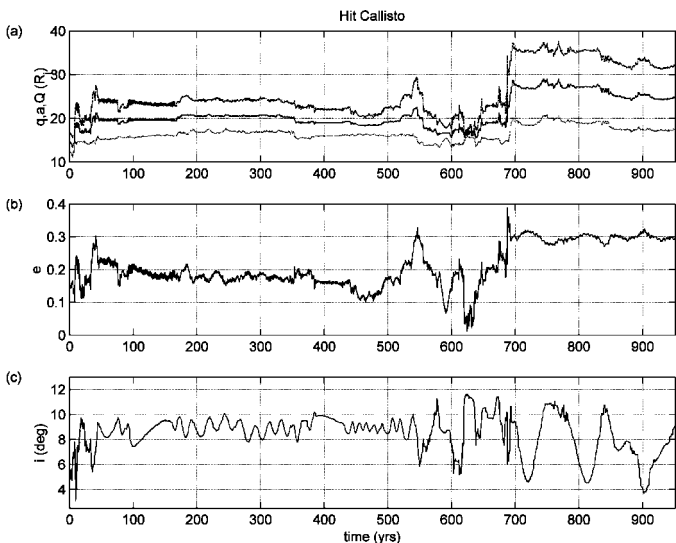


**FIG. 9.** Time history for a particle that hit Callisto. This particle was ejected at  $\zeta = 45^\circ$  at a speed  $f = 1.20$  and hit Callisto  $\sim 951$  years after launch. It got trapped in several resonances with Ganymede, namely the 2 : 3, 5 : 8, and 5 : 7 resonances. Note how it also got briefly trapped in a 1 : 1 resonance with Callisto around  $t \sim 840$ . (a) Perijove, semimajor axis, and apojove distance. (b) Eccentricity. (c) Inclination from Jupiter's equator.

a brief nonresonant period between 75 and 92 years. Later it fell into a 5 : 8 resonance with Ganymede from 180 to 320 years ( $\langle a \rangle \sim 20.5 R_J$ ). From 360 to 430 years it was in a 5 : 7 resonance with Ganymede ( $\langle a \rangle \sim 19.0 R_J$ ). The orbit then wandered chaotically for several years, falling into Callisto's chaotic zone (spanning between 23.9 and 28.7  $R_J$ ) before being briefly trapped in a 1 : 1 resonance (at 26.4  $R_J$ , from 835 to 845 years). Finally it hit Callisto at  $t = 951$  years.

We now concentrate on the particles that hit Ganymede (787 of 1067, or  $\sim 74\%$  of the total). As we have already seen, there are three kinds of behavior: (i) low-speed ejecta follow suborbital trajectories, (ii) slightly faster particles go into temporary orbits about Ganymede, and (iii) the fastest particles go into orbit about Jupiter. In Fig. 10a we show a histogram of the number of impacts vs logarithm of time. The minimum at  $t \sim 0.1$  years ( $\sim 37$  days, also visible as a gap in fig. 10b) suggests a natural division into two distinct groups of early and late impactors. In Fig. 10b we show the cumulative number of impacts on Ganymede as a function of time. Ejecta on suborbital trajectories impact in a few minutes to a couple of days. The open circles shown in Fig. 1 that stay close to the predictions of the time-of-free-flight formula (Eq. (2)) exemplify this suborbital behavior. At the other extreme there are particles that go into joventric orbits, later to impact Ganymede thousands of years after launch. Of the 686 particles that hit Ganymede

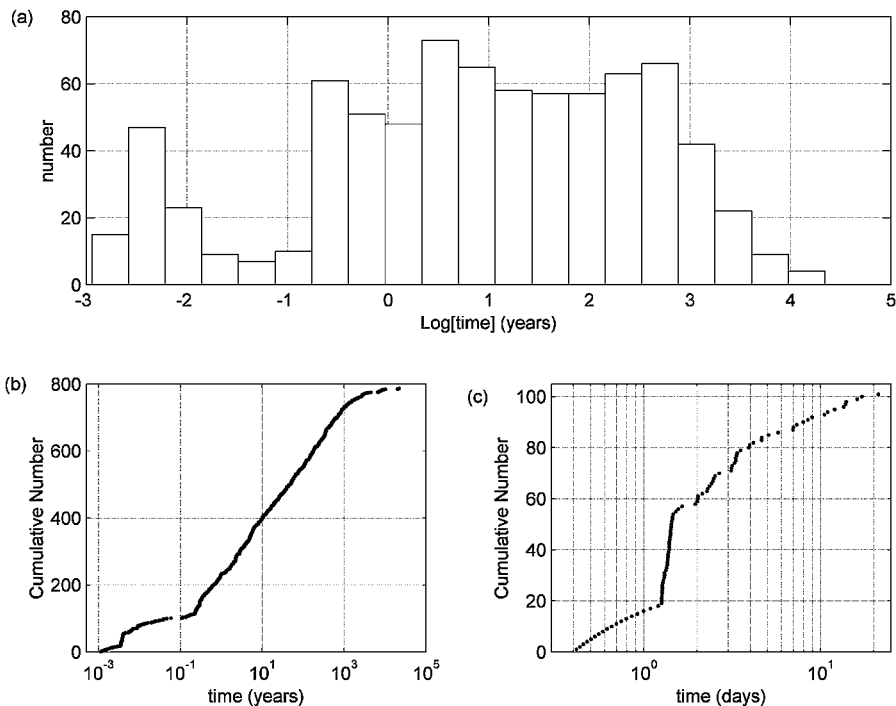


**FIG. 10.** Impacts on Ganymede. (a) Histogram of the number of impacts on Ganymede vs logarithm of time (years); there are clearly at least two groups, the dividing time being  $\sim 0.1$  years ( $\sim 37$  days). (b) Cumulative total number of impacts on Ganymede as a function of time. For the later impactors (see text), the number of hits seems to increase logarithmically: a least-squares fit gives  $N \approx 71 \log t + 231$ . (c) Number of impacts on Ganymede as a function of time such that the impacts occurred less than 37 days after launch (101 in total). Some of these particles were on suborbital trajectories (impact times less than  $\sim 1.6$  days) and some were temporarily in orbit around Ganymede before impact. Note that the time axis is in days.

TABLE VI

Number and Fraction of Particles Reaccreted within 0.1 Years ( $\sim 37$  Days) after Launch as a Function of Ejection Speed for Cases 2, 3, and 4 (Zenith Angles  $30^\circ$ ,  $45^\circ$ , and  $60^\circ$  Respectively)

Ejection speed, $f$	Number of particles re-accreting within 37 days	Fraction (out of a total of 180)
0.96	63	0.35
0.98	15	0.08
1.00	2	0.01
1.20	0	0.00

after 37 days, 630 (92%) hit within 1000 years. The cumulative number of impacts on Ganymede increases logarithmically in time for the span  $0.1 < t < 1,000$  years, i.e.,  $N = a \ln t + b$ . Least-squares fit to this range gives  $a \approx 71$ ,  $b \approx 231$ . This implies an accretion rate  $\dot{N} \approx 71/t$ : after one year, Ganymede was accumulating jovicentric objects at a rate of  $\sim 71/\text{year}$ , while at  $t = 1000$  years it was accumulating at the much lower rate of 0.071 objects per year (i.e., 1 object every 14 years). In Fig. 10c we show the cumulative number of impacts on Ganymede as a function of time for the 101 early impactors. The first 18 points draw a smooth curve which represents the suborbital particles ejected radially. The nearly vertical line is drawn by suborbital particles ejected at nonzero zenith angles. Particles that take between  $\sim 1.6$  and  $\sim 37$  days to impact show a different trend and represent the transition between the suborbital and the jovicentric impactors. These are particles that were briefly trapped into highly perturbed orbits around Ganymede before hitting it. All zenith angles are represented in Fig. 10c, while the speeds of the particles in the transition group roughly span the range  $0.96 < f < 1.00$ . The particle shown in Fig. 3 exemplifies this type of behavior. Evidently the early impactors consist of both suborbital ejecta and short-lived satellites. In Table VI we list the number and fraction of particles that were reaccreted within 0.1 years for Cases 2, 3, and 4 as a function of ejection speed.

As the speed of the ejecta increases, the chances of being quickly (0.1 years) reaccreted into Ganymede decrease, since the probability of escaping to jovicentric space increases. Let us use the circular restricted three-body problem (CR3BP henceforth; Szebehely 1967) as a model to analyze the Jupiter–Ganymede–particle system. In the CR3BP, two massive bodies move around their common center of mass in circular orbits, while a third, massless test particle experiences the gravitational attraction of the two massive bodies but does not itself influence their motion. The Jacobi constant defines regions of space forbidden to the test particle, i.e., the zero-velocity surface. For low speeds ( $f \ll 1.00$ ) the zero-velocity surface is a closed oval surrounding Ganymede. For higher speeds the zero-velocity oval inflates until its radius approaches the Hill radius ( $\sim 12.04 R_G$ ), at which point the oval opens through the  $L_2$  point. We show in the Appendix that to reach the Hill radius from the surface of Ganymede we must launch ejecta at the speed  $f_c \sim 0.96$ . It is approximately at

this critical speed that the zero-velocity surface starts to open and some ejecta are able to reach jovicentric space. An opening in the oval is a necessary, but not a sufficient condition for escape. Particles on chaotic orbits, however, will have a tendency to explore much if not all of the available phase space, and so these will eventually either collide with Ganymede or find a way out. Smith and Szebehely (1992) have shown that there is an onset of chaotic motion in the CR3BP when the surface of zero velocity starts to open. In addition Murison (1989) has demonstrated that the process of satellite capture, which is the problem of escape but time-reversed, has fractal properties resulting in chaotic motion: satellite capture or escape can occur only when the zero-velocity surface is open. The complexity of an orbit such as the one shown in Fig. 3, where the ejection speed is close to the critical value  $f_c$ , and the studies of Murison and Smith and Szebehely lead us to strongly suspect that the subsatellites temporarily orbiting Ganymede are chaotic. The higher the ejection speed, the wider the opening, and the greater the probability that transitional objects will find the hole in the oval and escape. This is why in Table VI the fraction of particles that are quickly reaccreted decreases as we increase the ejection speed. While there is no sharp dividing line for escape to jovicentric space, there is a transition region of temporary satellites that could form a short-lived cloud of debris surrounding Ganymede after a major impact.

Repeated close encounters and mean-motion resonances (mostly with Ganymede) drive the dynamics of the jovicentric particles. Eventually they impact in time frames ranging from a few months to a few thousand years. The time scales are consistent with those obtained by Horedt and Neukum (1984), who for example give a mean time interval for collisions with Ganymede of 1200 years for a particle with eccentricity  $e = 0.6$ , inclination  $i \sim 15^\circ$ . Lower eccentricities and lower inclinations have lower lifetimes. In Fig. 11 we show a particle that hit Ganymede after orbiting Jupiter for 671 years. This particle was launched radially from Gilgamesh at a speed  $f = 1.329$ ; it gets temporarily trapped in many resonances with Ganymede as evidenced by the behavior of the semimajor axis. From 51 to 135 years, its average semimajor is  $\langle a \rangle = 19.6 R_J$ , meaning it is captured into a 2 : 3 resonance with Ganymede. Then, from 215 to 252 years,  $\langle a \rangle = 17.4 R_J$ , so that it is captured into a 4 : 5 resonance with Ganymede. Around  $t \sim 295$  years the particle suffers a close approach to Ganymede, when its semimajor axis increased from 16 to  $20 R_J$  and its eccentricity jumped from  $\sim 0.03$  to 0.23. Around the time of this close encounter, the semimajor axis dipped into Ganymede’s chaotic zone (between  $13.5$  and  $16.5 R_J$ ). This close encounter affected the inclination as well. Prior to this close encounter the mean inclination was  $9^\circ$ , while after the close encounter the mean inclination dropped to about  $5^\circ$ . From 397 to 419 years the particle returns to the 4 : 5 resonance with Ganymede. Finally at  $t \sim 657$  years the particle reenters Ganymede’s chaotic zone, impacting Ganymede 671 years after launch.

The behavior of the particles that hit Io is rather similar to those hitting Europa, Ganymede, or Callisto. Any particle

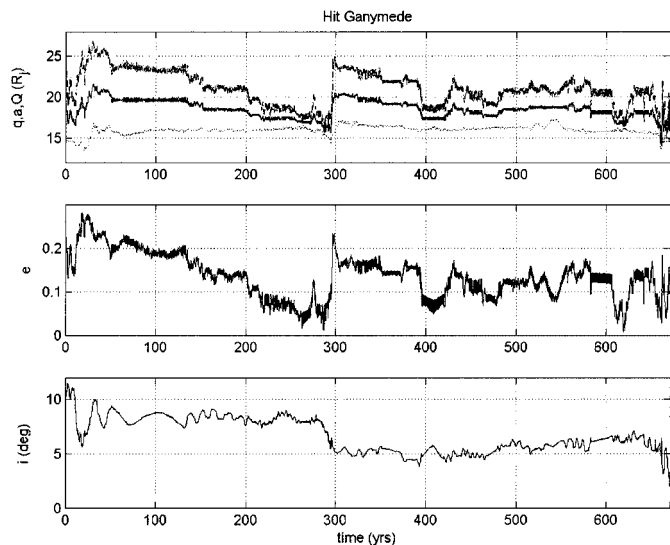


FIG. 11. Time history for a particle that hit Ganymede. This particle was ejected at a speed  $f = 1.20$  and impacted  $\sim 671$  years after launch. (a) Perijove, semimajor axis, and apoapse distance. (b) Eccentricity. (c) Inclination from Jupiter's equator. Note how this particle gets trapped into numerous resonances with Ganymede. It also dips into Ganymede's chaotic zone twice: once around  $t = 295$  years and then again around  $t = 657$  years.

in a mean-motion resonance with any of the three innermost Galilean moons is also in a resonance with the other two due to the Laplace resonance involving Io, Europa, and Ganymede (Murray and Dermott 1999). Io is in a 2:1 mean-motion resonance with Europa, which is itself also in a 2:1 resonance with Ganymede. For example, we saw how the particle shown in Fig. 11 twice became temporarily trapped in a 4:5 resonance with Ganymede; at the same time this particle was also in a 2:5 resonance with Europa and in a 1:5 resonance with Io.

Partitioning between the various fates (Ganymede, Europa, Jupiter, etc.) is not a strong function of ejection speed. In Fig. 12 we show a 3-D bar graph which bins the fates of the jovicentric ejecta according to ejection speed. We combine the cases  $\zeta = 30^\circ$ ,  $45^\circ$ , and  $60^\circ$  and omit the radial ejecta from this figure. Of the total of 900 ejecta particles, 820 were jovicentric. The percentages shown refer to the number of jovicentric particles at a given speed. For example, at  $f = 1.00$ , there were 178 jovicentric particles, of which 135 hit Ganymede (76%). Ganymede is the major sink at all speeds; however, the probabilities of hitting something other than Ganymede (mostly Europa or Callisto) increase at higher speeds; this is consistent with what we have already seen in Fig. 1. The fraction of particles impacting Io increases up until  $f = 1.20$ , then decreases slightly. The fraction of particles that escape to heliocentric space increases sharply at  $f = 1.40$ . Too few particles struck Jupiter (3 cases) to allow any generalizations.

In Fig. 13 we show the fates of all the jovicentric ejecta as a function of zenith angle. Here include the radial ejecta ( $\zeta = 0^\circ$ ) and combine all speeds and azimuths. As in Fig. 12, the percent-

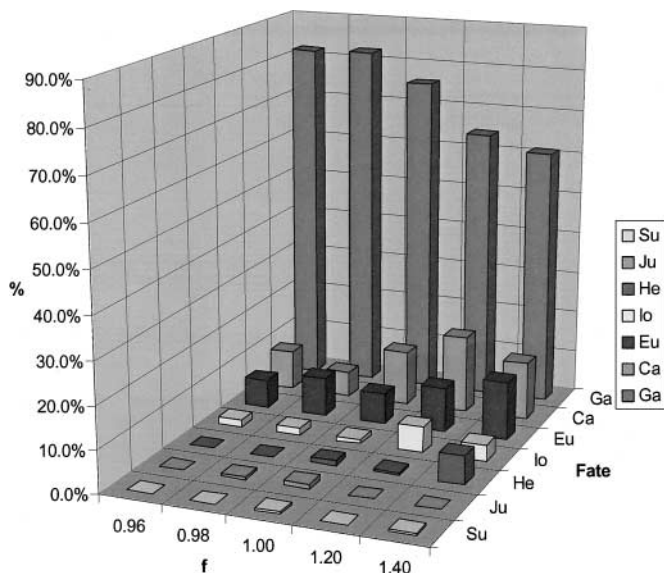


FIG. 12. Bar graph showing the fates of the jovicentric ejecta as a function of ejection speed. We have only included the cases  $\zeta = 30^\circ$ ,  $45^\circ$ , and  $60^\circ$  here (a total of 820 particles). Adding the percentages at a given speed gives 100%. It is apparent that at higher speeds, the probability of being swept up by Ganymede decreases. Note how at faster speeds the **Ga**(nymede) bars get shorter, while the **Eu**(ropa) and **Ca**(listo) bars get taller. This is consistent with the results shown in Fig. 1, where we plotted the fate of each particle as a function of speed for the radial case ( $\zeta = 0^\circ$ ). **Ga**, Ganymede; **Ca**, Callisto; **Eu**, Europa; **Su**, survivors; **Io**, self; **He**, heliocentric escapes; **Ju**, Jupiter.

ages shown are relative to the total number of jovicentric cases at a given zenith angle. There is no strong trend; it may be that the probability of impacting with Ganymede increases slightly at higher zenith angles.

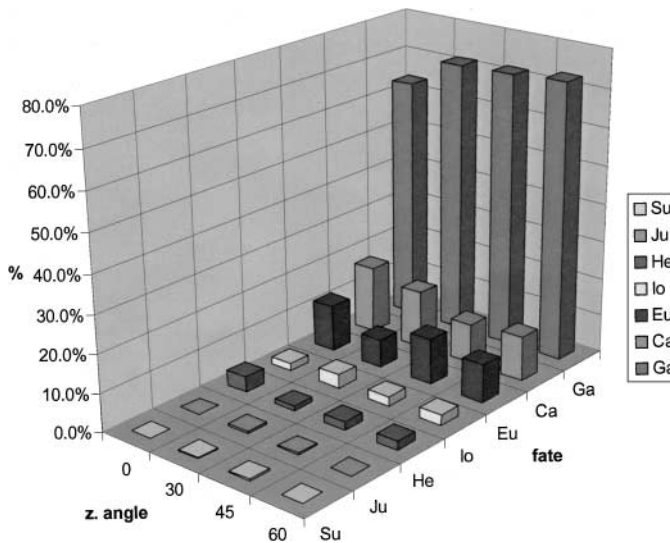


FIG. 13. Bar graph showing the fates of the jovicentric ejecta as a function of the ejection zenith angle. Radial ejecta are included as the  $\zeta = 0^\circ$  case. A total of 966 cases are represented here. Adding the percentages at a given zenith angle gives 100%. It seems that the probability of being swept up by Ganymede increases slightly with increasing zenith angle. **Ga**, Ganymede; **Ca**, Callisto; **Eu**, Europa; **Su**, survivors; **Io**, self; **He**, heliocentric escapes; **Ju**, Jupiter.

TABLE VII  
Fate of the Jovicentric Ejecta (Particles That Hit Ganymede in Less Than 37 Days Are Not Included Here) after  $10^5$  Years

Fate	Total	% of total jovicentric cases
Hit Jupiter	3	0.3
Hit Io	28	2.9
Hit Europa	98	10.1
Hit Ganymede	686	71.0
Hit Callisto	128	13.3
Heliocentric	21	2.2
Survivors	2	0.2
Total	966	100.00

In Table VII we summarize our results. Only the particles that achieved jovicentric orbits are included in this table. For the particles that hit Ganymede we include only those that impacted more than 37 days after launch (which we assume to be in prograde, jovicentric orbits).

## V. IMPACTS ON THE GALILEAN SATELLITES

According to Horedt and Neukum (1984), “when satellites are cratered by planetocentric projectiles of moderate eccentricity, no marked crater frequency asymmetry is expected because the relative velocity between projectile and satellite is approximately symmetric with respect to the satellite’s circular orbital velocity.” In other words, we expect the distribution of impact sites from these planetocentric impactors to be random on prograde, synchronously rotating satellites such as Ganymede. We wish to measure the impact locations of the returning particles. When SWIFT removes a particle it writes a file that contains a snapshot of the system at that moment. In general the removed particle is either a few Ganymede radii away from Ganymede or actually inside of it. To find out where on Ganymede these particles hit, we wrote a program that takes as input this snapshot file from SWIFT, identifies which particles were removed by Ganymede, and integrates them until they hit the surface. For this purpose we used the CR3BP. (Szebehely, 1967) to describe the particle, Ganymede, and Jupiter. We integrate the CR3BP equations of motion using a Bulirsch–Stoer method (Press *et al.* 1986) until the particle intersects the surface of Ganymede. SWIFT usually removes particles while they are inside Ganymede’s Hill sphere, so we only need to integrate for a few tens of minutes before they actually hit. The approximations here are that during this short time Ganymede is traveling in a perfectly circular orbit (Ganymede’s forced eccentricity is 0.0015) and that the only forces acting on the particle are Jupiter’s and Ganymede’s gravitational attractions. We then use linear interpolation to find where on the surface the impactor hit.

In Fig. 14 we plot the impact sites for the early impactors (the suborbital and temporary satellites). There is a chain of secondary craters originating at Gilgamesh (oval centered on  $237^\circ, -58^\circ$ ) and moving leftward and upward; the rotation of

Ganymede makes the chain move to the left (westward), while the attraction of Jupiter makes the chain curve northward. This chain is an artifact of vertical launch and was produced by the same 18 particles shown in Fig. 1 that obey the time-of-free-flight formula (Eq. (2)). Impact sites of slower conical ejecta (ejected at  $f = 0.96, 0.98$ ) also form regular patterns such as loops and chains. For more details on the impact characteristics of suborbital ejecta see Dobrovolskis (1981). The rest of the impact sites shown in this figure are formed by the debris that became temporary chaotic satellites of Ganymede. There appears to be a small bias toward the northern hemisphere, perhaps because Gilgamesh is located in the southern hemisphere.

Starting at the critical speed  $f_c \sim 0.96$ , the ejecta are increasingly able to escape to jovicentric space (see Table VI). In Fig. 15 we map on Ganymede where the impacts by jovicentric objects occurred. In Fig. 16a we plot a histogram of the impact longitudes of the jovicentric objects, which seem to be randomly oriented, although there seems to be a slight bias toward the trailing hemisphere. These impacts are produced by prograde jovicentric impactors, and so we should not expect to see any large asymmetry between the leading and trailing sides in the crater counts. Fig. 16b shows a histogram of the impact latitudes; the solid curve is a plot of cosine of latitude. Most of the impacts indeed occur close to the equator, as would be expected for isotropic impactors.

To quantify the degree of cratering asymmetry produced by heliocentric impactors, Zahnle *et al.* (2001) defined a global measure of apex–antapex cratering asymmetry, or GMAACA, as the ratio of the number of craters that fall within  $30^\circ$  of the apex of motion (i.e., in the leading hemisphere) to the number of craters that fall within  $30^\circ$  of the antapex. Their Monte Carlo

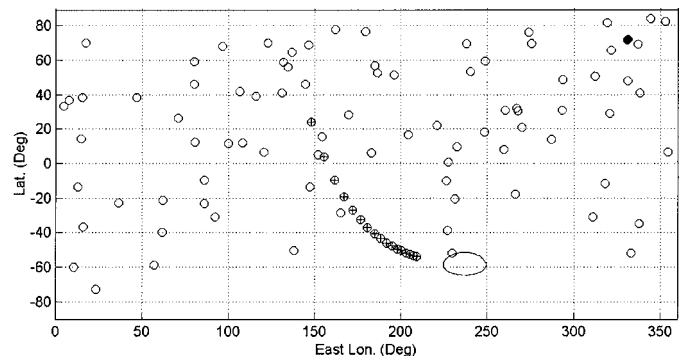


FIG. 14. Impact sites on Ganymede for impacts occurring in less than 37 days (101 cases). The sub-Jupiter point is located at the origin. The trailing hemisphere runs from 0 to 180 degrees; the leading one ranges from longitudes 180 to 360 degrees. The oval centered at  $(237^\circ, -58^\circ)$  represents the outline of Gilgamesh (600 km across). Some of these impact patterns are produced by particles on suborbital trajectories that impact Ganymede within a few hours after launch. Earth symbols ( $\oplus$ ) represent the impact sites of the 18 suborbital particles launched vertically, previously shown in Fig. 1. Other impact sites are produced by ejecta temporarily trapped in orbits around Ganymede; the filled circle at  $(331^\circ, +72^\circ)$  shows the impact location of the particle shown in Fig. 3, which is an example of this latter type.

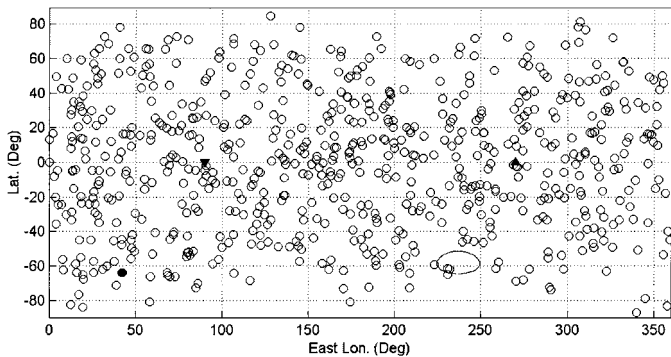


FIG. 15. Impact sites on Ganymede produced by joventric impactors. The sub-Jupiter point is located at the origin. The trailing hemisphere runs from 0 to 180 degrees; the leading one ranges from longitudes 180 to 360 degrees. The oval centered at  $(237^\circ, -53^\circ)$  represents the outline of Gilgamesh (600 km across). The upward-pointing triangle represents the apex of motion, while the downward-pointing triangle represents the antapex. Note the random location of the impact sites, consistent with planetocentric debris. The solid circle at  $(+42^\circ, -64^\circ)$  shows the impact location of the particle shown in Fig. 11.

studies suggest that, had the craters on Ganymede been produced exclusively by ecliptic/heliocentric comets, GMAACA should be on the order of 70; previous analytic studies (Shoemaker and Wolfe 1982) had indicated a range  $15 < \text{GMAACA} < 30$ . The observed GMAACA on Ganymede for craters bigger than 30 km diameter is approximately 4.3; i.e., there is an asymmetry, although it is much smaller than what is predicted for exclusively heliocentric impactors (Zahnle *et al.* 2001). Zahnle *et al.* estimated that what is observed on Ganymede can be explained as cratering by a population composed of roughly 50% ecliptic comets and 50% isotropic (i.e., joventric) impactors.

Given an object of diameter  $d$  (km), impacting at an incident speed  $v_{\text{inc}}$  ( $\text{km s}^{-1}$ ) at an incident angle  $\theta_{\text{inc}}$ , the diameter  $D$  (km)

of the resulting crater is given by (Zahnle *et al.* 2001)

$$D = D_0 (d^{0.78} v_{\text{inc}}^{0.44} \cos^{0.33} \theta_{\text{inc}})^\xi. \quad (5)$$

The coefficient  $D_0$  takes into account such factors as density and surface gravity while the exponent  $\xi$  takes into account crater slumping; for Ganymede these values are 4.23 km and 1.13 respectively (Zahnle *et al.* 2001). We draw an analogy to the asteroid Vesta to estimate the size and number of large blocks ejected into orbit about Jupiter during the excavation of Gilgamesh. About a score of 5- to 10-km-size blocks of Vesta are now independent asteroids in heliocentric orbit (Burbine *et al.* 2001); another 200 smaller Vestoids are known. It is likely that they were launched in the process of excavating a 460-km crater on Vesta, which itself has a diameter of about 525 km. According to Melosh (1989, p. 101), the largest secondary crater is typically about 4% the diameter of the primary, independent of the size of the primary. Gilgamesh is not substantially different in this regard; its largest secondary is 20 km wide (P. Schenk, personal communication). Therefore we assume that the largest block size is linearly proportional to the size of the crater. Melosh (1989, p. 105) also points out that the largest block size is inversely proportional to the ejection velocity. Hence we estimate that the largest escaping block scales as  $D_{\text{pr}}/v_{\text{esc}}$ , where  $D_{\text{pr}}$  is the primary crater's diameter. The escape velocity from Vesta is  $0.36 \text{ km s}^{-1}$  and to escape from Ganymede we must launch at  $f_c v_{\text{esc}} \sim 2.63 \text{ km s}^{-1}$ . Hence we estimate that Gilgamesh launched about a score of 0.9- to 1.8-km blocks, and a larger number of smaller ones, into orbit about Jupiter.

In Fig. 17 we plot the incident speeds and angles for the joventric objects that hit Ganymede as a function of time. The incident speeds generally increase with time, while the incident

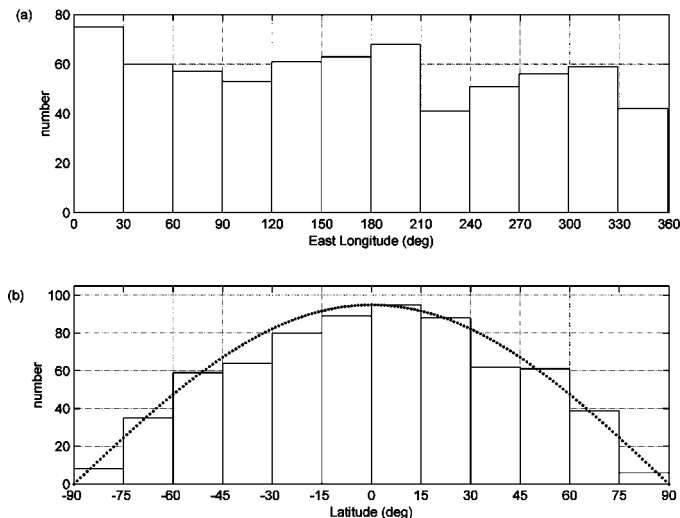


FIG. 16. (a) Histogram on the impact longitudes for the joventric impactors shown in Fig. 14; bin size is 15 degrees. (b) Histogram of the impact latitudes for the joventric impactors shown in Fig. 15. The curve shown represents the cosine of latitude; bin size is 30 degrees.

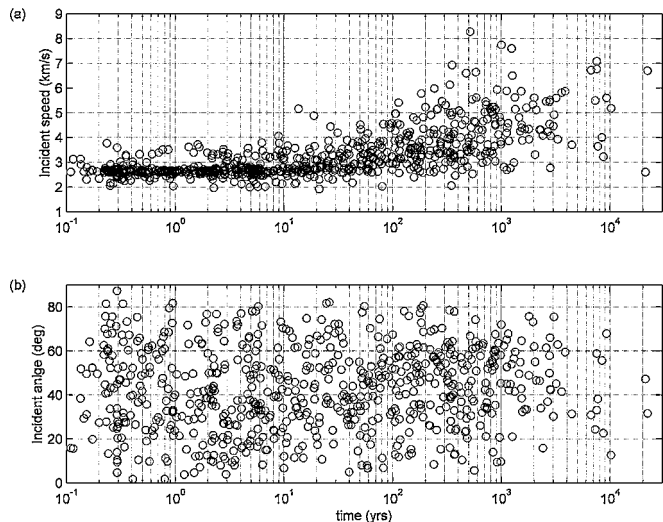


FIG. 17. (a) Incident impact speeds with Ganymede due to joventric objects as a function of time; note how the incident speed increases with time on average. (b) Incident impact angle with Ganymede due to joventric objects as a function of time; the values are normally distributed between 0 and 90 degrees.

angles are isotropically distributed between  $0^\circ$  and  $90^\circ$ . The fastest impact speed shown in Fig. 17 is  $8.3 \text{ km s}^{-1}$ . If we take as the largest block size  $d_{\text{max}} \sim 1.8 \text{ km}$  and  $\theta_{\text{inc}} = 0^\circ$ , we obtain that the largest possible crater is  $D_{\text{max}} \sim 20 \text{ km}$  across. A more typical crater produced by jovian debris would be produced by a block a few hundred meters across, with an incident speed of  $3\text{--}4 \text{ km s}^{-1}$  and impacting at an incident angle of  $45^\circ$  to the local vertical. The resulting crater would be a few kilometers wide. Most of the craters shown in Fig. 15 would be of roughly this size and smaller, with about a score of 6- to 12-km craters (from the score of 0.9- to 1.8-km blocks). These ejecta cannot provide an explanation for the observed dilution of the predicted asymmetry for the larger ( $D > 30 \text{ km}$ ) craters. Hence Zahnle *et al.* (2001) favor nonsynchronous rotation for Ganymede sometime in the past.

Similar arguments can be applied to Europa, where the largest impact craters are on the order of 30- to 50-km diameter, and  $v_{\text{esc}} = 2.0 \text{ km s}^{-1}$ . For European craters we use the values  $D_0 = 4.64 \text{ km}$  and  $\xi = 1.09$  in Eq. (5) (Zahnle *et al.* 2001). We therefore expect that scores of 100-m-size blocks were launched into jovian orbit to yield scores of exalted secondaries in the 0.5- to 1-km diameter size range and many more that are smaller. Note also that the debris does not need to come from Europa itself.

Finally in Fig. 18 we show the impact speeds of the planetocentric test particles with Io, Europa, and Callisto vs. time. These numbers were obtained by the same method as was used in the case of Ganymede. In general, impact speeds on the inner moons are greater than on Callisto. Major impact events are capable of exporting surface materials to other moons. For example, silicates or carbonaceous materials from Ganymede or Callisto can be transferred to Europa. It is also reasonable

to suppose that sulfur can be sent from Io to Europa, where it would be oxidized to sulfate if it were not oxidized already. It is also possible to send ice to Io, where it might be welcomed. We crudely assume that an impact on Ganymede should launch at escape velocity an amount of ejecta comparable to (or somewhat greater than) the mass of the impactor itself. This takes into account both the excavation flow (with maximum velocities some 10–20% that of the impact velocity, and thus comparable to the escape velocity) and the more complicated interactions involving the impactor and the comparable mass of target material that it directly strikes. Escape from Europa would be somewhat easier, and escape from Callisto would be somewhat more difficult. We have found in this study that about 13% of the ejecta that escape Ganymede reach Callisto, another 10% reach Europa, and 3% reach Io. The planetocentric volatile source is probably somewhat smaller (by mass) than direct impacts by comets; however, the planetocentric impact velocities are so much smaller that the planetocentric source is likely to be the more important.

As a specific example consider the transfer of water from Ganymede and Europa to Io. It is reasonable to guess that an impact event on Europa capable of producing a Gilgamesh-type crater could also transfer to Io  $\sim 10\%$  of the impact ejecta, but the transfer rate for a similar event on Callisto would be less than 3%. Overall we would expect that the planetocentric source of water ice to Io would be more than 10% of the source from direct cometary impacts. When we consider the relative impact velocities ( $25\text{--}40 \text{ km s}^{-1}$  for comets, rather than  $3\text{--}7 \text{ km s}^{-1}$  for planetocentric debris) it is obvious that the planetocentric source is probably Io's greatest net source of water. A kilometer-size comet (if they exist in numbers predicted by a power-law fit to larger comets) strikes Europa or Ganymede about once every one or two million years (Zahnle *et al.* 1998). Hence the net source of water for Io from this process is probably on the order of  $10^{10} \text{ kg year}^{-1}$ . One can make similar estimates regarding transfer of sulfur from Io to Europa or of dry ice from Callisto to Ganymede (etc.) given knowledge of surface compositions; these will be fraught with uncertainty, but when impact velocities are taken into account they are not likely to be smaller than what one would guess is falling from comets directly.

## VI. SUMMARY

We have simulated the dynamical evolution of fast impact ejecta in the jovian environment. We took as the source of the ejecta the giant impact basin Gilgamesh, located on the leading hemisphere of Ganymede. The simulation consisted of over 1000 test particles, Jupiter (plus its two leading oblateness terms), the Galilean moons, Saturn, and the Sun, all integrated for  $10^5$  years using the SWIFT integrator of Levison and Duncan. The slower ejecta ( $f < 0.96$ ) follow suborbital trajectories. Starting at the critical speed  $f_c \sim 0.96$ , there is a qualitative change in the nature of the ejecta trajectories and more complex behavior appears. As the critical speed is reached the surface of zero velocity surrounding Ganymede begins to open through

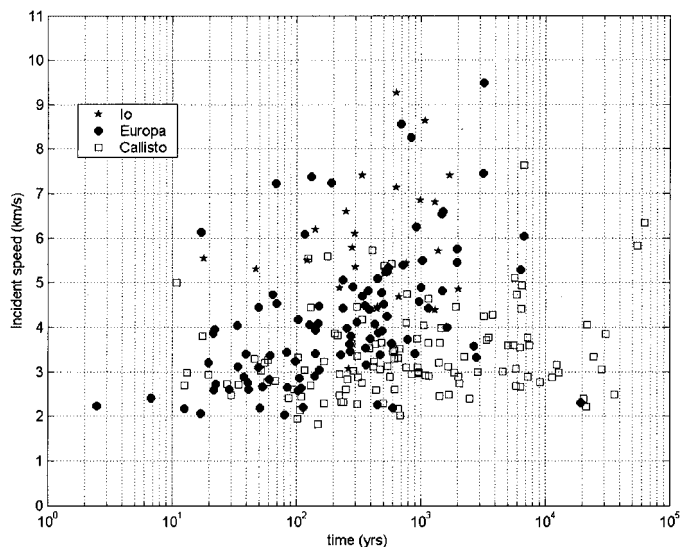


FIG. 18. Incident impact speeds of the planetocentric debris with Io, Europa, and Callisto as a function of time; again, the incident speed increases with time on average.

the  $L_2$  point and the trajectories display symptoms of chaotic behavior. Some of these chaotic ejecta achieve temporary orbits about Ganymede. These particles represent the transition between the low-energy, suborbital trajectories and the more energetic ejecta that reach joventric orbits. Above the critical value  $f_c$ , the greater the speed, the greater the fraction of particles able to escape to joventric space. Approximately  $\sim 71\%$  of the ejecta that reached joventric orbits eventually were reaccreted by Ganymede, with  $92\%$  of the reaccretions occurring within 1000 years. During this time the rate of particle accretion scales as  $t^{-1}$ . Impact sites on Ganymede are randomly distributed, as expected for prograde, planetocentric debris. However, the likely small size of these fragments ( $\sim 2$  km at most), coupled with their relatively low impact velocities (typically  $\sim 3\text{--}4$  km  $\text{s}^{-1}$ ), makes it unlikely that ejecta from Gilgamesh could account for the dilution of the expected apex–antapex asymmetry of large ( $D > 30$  km) craters observed on Ganymede. Of the rest of the escaping ejecta particles, about  $10\%$  hit Europa, some  $13\%$  hit Callisto, and  $3\%$  hit Io. Major impact events are capable of exporting surface materials to other satellites. We have estimated the size of the resulting craters on Europa to be 1 km and smaller. Only about  $2\%$  of the ejecta escaped to heliocentric space, while less than  $1\%$  reached Jupiter. Only two particles survived the  $10^5$ -year integration, but these do not appear to show signs of long-term stability.

## APPENDIX

### The Rotation of Ganymede and Derivation of the Critical Speed $f_c$

Consider a new coordinate system consisting of a nonrotating frame centered on Ganymede ( $x_0, y_0, z_0$ ). The speed of the particles in this new sidereal frame is (Dobrovolskis 1981)

$$v_0^2 = v^2 + b^2 + 2vb \sin \zeta \sin \alpha, \quad (\text{A1})$$

where  $v$  is the speed in the body-fixed frame,  $b = \omega R_G \sin \theta$  is the rotational speed at co-latitude  $\theta$ ,  $\omega$  is Ganymede's angular rotational speed, and  $R_G$  is its radius. It is clear that, in parallel to Eq. (1), we can also define a "sidereal"  $f_0$  in this frame such that  $v_0 = f_0 v_{\text{esc}}$ . At the same time, we can define a new inertial zenith angle  $\zeta_0$  which is related to the zenith angle measured from the local vertical  $\zeta$  by the equation (Dobrovolskis 1981)

$$\cos \zeta_0 = (v/v_0) \cos \zeta. \quad (\text{A2})$$

To obtain the speed needed to reach the Hill radius (i.e., the critical speed) we proceed as follows. The semimajor axis with respect to Ganymede of the ejected particle  $a$  can be obtained from its specific energy at launch, so that using  $v_0 = f_0 v_{\text{esc}}$  and solving for the semimajor axis  $a$  we obtain

$$a = \frac{R_G}{2(1 - f_0^2)}. \quad (\text{A3})$$

The eccentricity of the ejected particle can be obtained from its semilatus rectum,  $p = a(1 - e^2) = h^2/GM_G$  (Danby 1992, p. 128), where  $h$  is the specific angular momentum, which can be written as  $h = R_G v_0 \sin \zeta_0$ . Using Eq. (A3)

to eliminate the semimajor axis and solving for  $e$  we obtain

$$e^2 = 1 - 4f_0^2(1 - f_0^2) \sin^2 \zeta_0. \quad (\text{A4})$$

The apoapse distance is  $Q = a(1 + e)$ ; substituting Eqs. (A3) and (A4) into this we obtain  $Q$  as a function of  $f_0$  and  $\zeta_0$ :

$$Q = \frac{R_G}{2(1 - f_0^2)} \left[ 1 + \sqrt{1 - 4f_0^2(1 - f_0^2) \sin^2 \zeta_0} \right]. \quad (\text{A5})$$

We wish to find a value of  $f_0$  at which the apoapse of the ejected particle will equal Ganymede's Hill radius, i.e.,  $R_H = a_G(M_G/3(M_G + M_J))^{1/3}$ . Hence we set  $Q = R_H$  and solve for the critical value of  $f_0$ , to obtain

$$f_c = \sqrt{\frac{R_H^2 - R_H R_G}{R_H^2 - R_G^2 \sin^2 \zeta_0}}. \quad (\text{A6})$$

For Ganymede,  $R_H \sim 12.04 R_G$ , so Eq. (A6) gives  $f_c \sim 0.95757$  for  $\zeta_0 = 0^\circ$  and  $f_c \sim 0.96089$  for  $\zeta_0 = 90^\circ$ . Thus, the critical launch speed is insensitive to the launch angle. For fast particles ejected out of slowly rotating bodies (i.e.,  $v \gg b$ ), which are the cases we consider here, we can safely ignore the speed due to rotation. For example, Ganymede's period of rotation is 7.155 days, so that  $b \cong 27 \sin \theta \text{ m s}^{-1}$ . Since we are mostly interested in particles that escape,  $\omega R_G \sin \theta$  is at most  $\sim 1\%$  of Ganymede's escape speed of  $2.74 \text{ km s}^{-1}$ . Hence for all the cases we consider in this paper,  $v \cong v_0$  and therefore we can assume that  $\zeta \cong \zeta_0$  and  $f \cong f_0$ .

## ACKNOWLEDGMENTS

JLA and KJZ want to thank NASA's Exobiology program for support, while ARD acknowledges Planetary Geology and Geophysics for support. We also thank Luke Dones and Hal Levison for information on the use of SWIFT. The authors also thank Boris Ivanov and an anonymous referee for their reviews containing numerous helpful comments. We also thank Jack Lissauer for useful discussions. Finally JLA thanks Alejandra, Joselito, and Isabella for their patience while this project was under way. This research has made use of NASA's Astrophysics Data System (ADS located at <http://adswwww.harvard.edu>).

## REFERENCES

- Bate, R., D. Muller, and J. White 1971. *Fundamentals of Astrodynamics*. Dover, New York.
- Burbine, T. H., P. C. Buchanan, R. P. Binzel, S. J. Bus, T. Hiroi, J. L. Hinrichs, A. Meibom, and T. J. McCoy 2001. Vesta, Vestoids, and the howardite, eucrite, diogenite group: Relationships and the origin of spectral differences. *Meteorit. Planet. Sci.* **36**, 761–781.
- Burns, J. A., and B. J. Gladman 1998. Dynamically depleted zones for Cassini's safe passage beyond Saturn's rings. *Planet. Space Sci.* **46**, 1401–1407.
- Burns, J. A., M. R. Showalter, and G. E. Morfill 1984. The ethereal rings of Jupiter and Saturn. In *Planetary Rings* (R. Greenberg and A. Brahic, Eds.), pp. 200–272. Univ. of Arizona Press, Tucson.
- Chapman, C., and W. McKinnon 1986. Cratering of planetary satellites. In *Satellites* (J. Burns and M. S. Mathews, Eds.), pp. 492–580. Univ. of Arizona Press, Tucson.
- Chirikov, B. V. 1979. A universal instability of many dimensional oscillator systems. *Phys. Rep.* **52**, 263–279.
- Cintala, M. J., J. W. Head, and L. Wilson 1979. The nature and effects of impact cratering on small bodies. In *Asteroids* (T. Gehrels, Ed.), pp. 579–600. Univ. Of Arizona Press, Tucson.

- Danby, J. M. A. 1992. *Fundamentals of Celestial Mechanics*. Willmann-Bell, Richmond, VA.
- Dobrovolskis, A. R. 1981. Ejecta patterns diagnostic of planetary rotations. *Icarus* **47**, 203–219.
- Dobrovolskis, A. R., and J. J. Lissauer 2000. The fate of ejecta from Hyperion. *Bull. Am. Astron. Soc.* **32**, 861.
- Dobrovolskis, A. R., J. L. Alvarillos, and K. Zahnle 2000. A dynamical survey of the jovian system. *Bull. Am. Astron. Soc.* **32**, 1116.
- Duncan, M., T. Quinn, and S. Tremaine 1989. The long-term evolution of orbits in the Solar System: A mapping approach. *Icarus* **82**, 402–418.
- Evans, N. W., and S. Tabachnik 1999. Possible long-lived asteroid belts in the inner Solar System. *Nature* **399**, 41–43.
- Farinella, P., A. Milani, A. M. Nobili, P. Paolicchi, and V. Zappala 1983. Hyperion: Collisional disruption of a resonant satellite. *Icarus* **54**, 353–360.
- Farinella, P., P. Paolicchi, R. G. Strom, J. S. Kargel, and V. Zappala 1990. The fate of Hyperion's fragments. *Icarus* **83**, 186–204.
- Farinella, P., C. Froeschlé, R. Gonczy, G. Hahn, A. Morbidelli, and G. B. Valsecchi 1994. Asteroids falling into the Sun. *Nature* **371**, 314–317.
- Farinella, P., F. Marzari, and S. Matteoli 1997. The disruption of Hyperion and the origin of Titan's atmosphere. *Astron. J.* **113**, 2312–2316.
- Gault, D. E., E. M. Shoemaker, and H. J. Moore 1963. *Spray Ejected from the Lunar Surface by Meteoroid Impact*. NASA TND-1767.
- Gladman, B. 1997. Destination: Earth. Martian meteorite delivery. *Icarus* **130**, 228–246.
- Gladman, B. J., J. A. Burns, M. J. Duncan, and H. F. Levison 1995. The dynamical evolution of lunar impact ejecta. *Icarus* **118**, 302–321.
- Horedt, G. P., and G. Neukum 1984. Planetocentric versus heliocentric impacts in the jovian and saturnian satellite systems. *J. Geophys. Res.* **89**, 10405–10410.
- Levison, H. F., and M. J. Duncan 1994. The long-term dynamical behavior of short period comets. *Icarus* **108**, 18–36.
- Lissauer, J., S. W. Squyres, and W. K. Hartmann 1988. Bombardment history of the Saturn system. *J. Geophys. Res.* **93**, 13776–13804.
- Melosh, H. J. 1989. *Impact Cratering: A Geological Process*. Oxford Univ. Press, New York.
- Mileikowsky, C., F. A. Cucinotta, J. W. Wilson, B. Gladman, G. Horneck, L. Lindegren, J. Melosh, H. Rickman, M. Valtonen, and J. Q. Zheng, 2000. Natural transfer of viable microbes in space. 1. From Mars to Earth and Earth to Mars. *Icarus* **145**, 391–427.
- Murison, M. 1989. The fractal dynamics of satellite capture in the circular restricted three-body problem. *Astron. J.* **98**, 2346–2359.
- Murray, C. D., and S. F. Dermott 1999. *Solar System Dynamics*. Cambridge Univ. Press, New York.
- Press, W. H., B. P. Flannery, S. A. Teukolsky, and W. T. Vetterling 1986. *Numerical Recipes: The Art of Scientific Computing*. Cambridge Univ. Press, Cambridge, UK.
- Shoemaker, E. M., and R. F. Wolfe 1982. Cratering time scales for the Galilean satellites. In *Satellites of Jupiter* (D. Morrison, Ed.), pp. 277–339. Univ. of Arizona Press, Tucson.
- Smith, B. A., and 28 colleagues 1982. A new look at the Saturn system: The Voyager 2 images. *Science* **215**, 504–537.
- Smith, R. H., and V. Szebehely 1992. The onset of chaotic motion in the restricted problem of three bodies. *Celest. Mech. Dynam. Astron.* **56**, 409–425.
- Strom, R. G., S. K. Croft, and J. M. Boyce 1990. The impact cratering record on Triton. *Science* **250**, 437–439.
- Szebehely, V. G. 1967. *Theory of Orbits*. Academic Press, New York.
- Wetherill, G. W. 1984. Orbital evolution of impact ejecta from Mars. *Meteoritics* **19**, 1–13.
- Wisdom, J. 1980. The resonance overlap criterion and the onset of stochastic behavior in the restricted three-body problem. *Astron. J.* **85**, 1122–1133.
- Wisdom, J., and M. Holman 1991. Symplectic maps for the n-body problem. *Astron. J.* **102**, 1528–1538.
- Zahnle, K., L. Dones, and H. F. Levison 1998. Cratering rates on the Galilean satellites. *Icarus* **136**, 202–222.
- Zahnle, K., P. Schenk, S. Sobieszczyk, L. Dones, and H. F. Levison 2001. Differential cratering of synchronously rotating satellites by ecliptic comets. *Icarus* **153**, 111–129.